

5th US Combustion Meeting
Organized by the Western States Section of the Combustion Institute
and Hosted by the University of California at San Diego
March 25-28, 2007.

Effects of Fuel Injection and Mixing on NO_x Performance of a Liquid-Fueled Stagnation Point Reverse Flow Combustor

P. Gopalakrishnan, P. Alison and J. M. Seitzman

*School of Aerospace Engineering, Georgia Institute of Technology,
Atlanta, Georgia, 30332-0150, USA*

The role of fuel-injection on the performance of a liquid-fueled (Jet-A) Stagnation Point Reverse Flow (SPRF) combustor is experimentally investigated. Chemiluminescence from CH* and OH* is imaged to visualize the heat release regions, while laser scattering from fuel droplets is employed to determine the distribution of liquid fuel in the combustor. The ratio of simultaneously acquired images of CH* and OH* chemiluminescence ratios are analyzed to obtain an estimate of the spatial distribution of burning-zone equivalence ratios in the combustor. While the overall flow features are similar to previous measurements of a gas fueled SPRF combustor, the combustion characteristics and NO_x performance in liquid-fueled operation are strongly controlled by fuel dispersion and evaporation. Distribution of liquid fuel inside the combustor is varied by traversing the fuel injector longitudinally within the co-annular air tube. It is found that injecting the liquid at the exit of the air annulus results in a highly lifted flame, similar to nonpremixed gaseous operation. This is attributed to the initial shielding of fuel from the high temperature return products for this injector placement. On the other hand, retracting the fuel injector well inside the air produces a more well-dispersed fuel pattern at the reactant inlet leading to a reduction of the equivalence ratio in the fuel consuming reaction zones. This results in a decrease in NO_x emissions when the liquid injector is retracted for the entire range of global equivalence ratios investigated.

1. Introduction

The performance of dry, low NO_x gas turbines, which employ lean premixed (or partially premixed) combustors, is often limited by static and dynamic combustor stability, power density limitations and expensive premixing hardware. To overcome these issues, a novel design, referred to as a Stagnation Point Reverse Flow (SPRF) combustor, has been developed. The combustor has been demonstrated to produce low NO_x and CO emissions while operating with both gaseous and liquid fuels [1]-[2]. The combustor consists of a tube with one end open and the other closed. Contrary to most combustors, the reactants and products enter and leave this combustor at the same (open) end. In the investigated configuration, the reactants are injected along the combustor centerline, while the products flow in the reverse direction to exit the combustor. Thus the outflowing products and inflowing reactants come into direct contact in a counterflow mixing/shear layer. The combustor has also been shown to operate stably over a wide range of flow rates and equivalence ratios. The geometry of the SPRF combustor ensures the existence of a low velocity (“stagnation”) region that acts to stabilize the flame. This coupled with the mixing of fuel and air with returning hot products and radicals allows this combustor to operate at very lean conditions over a range of loadings, without compromising stability [3]-[6].

In gas-fueled operation, comparable NO_x emissions were obtained for both premixed and nonpremixed modes. Comparison of the flowfields in the two modes of operation showed that the velocity fields are similar except in a small region close to the injector exit. In premixed operation, a weakly attached flame was obtained, with some combustion in the jet shear layer but most of the reaction occurring far downstream. In the nonpremixed mode, the flame is highly lifted and stabilized in the third quarter of the combustor, which is characterized by low mean velocities and high turbulence levels. Similarity in NO_x emissions for both operating modes has been attributed to efficient mixing of nearly all the fuel and air before burning. Since the fuel remains shielded from hot products by the coaxial air flow in nonpremixed operation, fuel and air internally premix to nearly the global equivalence ratio before combustion occurs [7].

Although gaseous fuels are suitable in many instances, a number of applications require burning liquid fuels effectively while producing low emissions, e.g. aircraft engines. Lean premixed, prevaporized combustion is one approach to achieve low NO_x emissions in liquid fueled systems. However, external prevaporization and premixing of liquid fuel presents a significant operational hazard and adds complexity to the system. Relatively low NO_x emissions have been achieved in the SPRF combustor with liquid fuels without external prevaporization through the use of a concentric injector design that relies on airblast atomization.

This paper describes the effects of liquid-dispersion and mixing on the NO_x performance and combustion characteristics of the SPRF combustor. This is investigated experimentally, primarily through application of non-intrusive optical diagnostic techniques such as chemiluminescence imaging, which acts as a marker of heat release rate [8]-[12], and laser scattering from fuel droplets, which provides information on liquid fuel distribution.

2. Experimental Set-Up

The SPRF combustor used in the current study is a laboratory scale, atmospheric pressure device. It consists of a concentric injector centrally located in a 70 mm inner diameter quartz tube, which is closed at the bottom end with a quartz disk. The base plate is fit snugly inside the quartz tube so that there is no measurable leakage of fuel/air through the closed end. A tri-concentric injector design is employed for liquid-fueled operation. The fuel is pumped through a 500 μm tube centered within a 6 mm tube with no flow in the outer region. The whole arrangement can be traversed inside a third concentric tube which forms an annular passage for air flow. The fuel tube is centered with respect to the outer air annulus using set-screws. The air stream surrounding the fuel facilitates atomization of the fuel jet. Care is also taken to ensure that the whole injector is centered with respect to the combustor. Air flow rate is monitored and controlled using a calibrated rotameter. The fuel flow rates are calculated based on measurements of excess oxygen in the product gases with a portable gas analyzer (Horiba CEMS-PG250). The gas analyzer also measures the NO_x emissions from the combustor. The temperature of the exhaust gas is monitored simultaneously with an unshielded K-type thermocouple. As the inlet air is not preheated, the combustor is ignited with a premixed mixture of natural gas and air and the liquid fuel is introduced gradually before switching to fully liquid operation. In this study, two separate fuel tube locations have been investigated – (1) liquid fuel injector is flush with the exit of the air injector (Flush case) and (2) liquid fuel injector is retracted to 3.25” above the exit of the air injector (Retracted case).

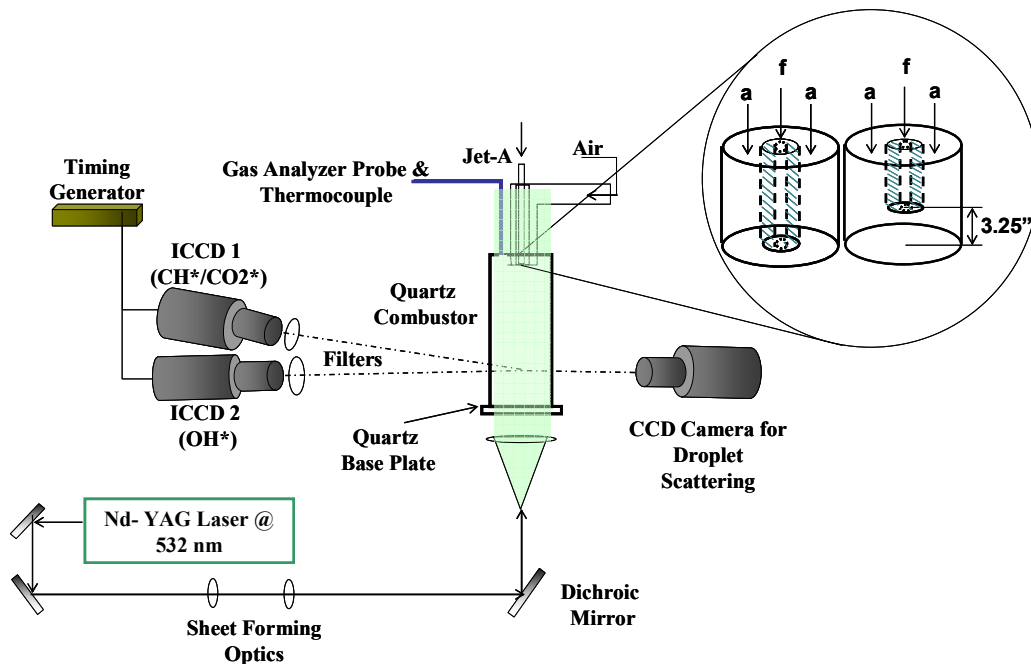


Figure 1. Experimental set-up for droplet scattering and $\text{CH}^*/\text{CO}_2^*/\text{OH}^*$ chemiluminescence imaging.

Chemiluminescence and Laser Scattering Systems

In this study, an intensified camera (18 mm intensifier, 384×576 pixels) with a 430 ± 5 nm filter placed in front of the lens is used to collect CH^* chemiluminescence and a portion of the CO_2^* chemiluminescence that occurs in the same spectral region (Figure 1). The distribution of liquid fuel in the combustor is visualized by illuminating the fuel jet with a laser light sheet produced from the 2nd harmonic output of a dual-head, pulsed Nd:YAG laser. The laser beam is converted into a thin sheet (~ 0.4 mm thick) 65 mm wide with two cylindrical lenses and enters the combustor from the closed end. The scattered light is detected normal to the laser sheet with a 12-bit interline CCD camera (1300×1030 pixels) and a 55 mm, $f/1.8$ camera lens. The intensifier gate of the chemiluminescence camera is synchronized with the droplet scattering system, such that the exposure begins 100 ns after the Nd:YAG laser pulse and lasts ~ 250 μs . Thus nearly simultaneous imaging of fuel droplets and chemiluminescence is achieved.

A second intensified camera (1024×256 pixels) equipped with a UV-Nikkor lens (105mm, $f/4.5$) and a WG308 Schott glass filter is used to obtain OH^* chemiluminescence measurements. The CH^* - CO_2^* chemiluminescence is imaged with the same imaging described previously. During this experiment, the droplet scattering system is disabled and the two intensified cameras are synchronized with a pulse generator. The cameras are aligned such that the angle between them is as small as possible and their fields of view are matched so as to obtain instantaneous imaging of CH^* and OH^* chemiluminescence over the entire volume of the combustor.

3. Results and Discussion

As noted earlier, one of the key features of the SPRF combustor is its ability to run stably over a range of equivalence ratios and loadings while producing ultra low NO_x emissions with both gaseous and liquid fuels. Figure 2 shows a comparison of the NO_x emissions obtained with

(liquid) Jet-A and natural gas fuels. Several similarities are seen between the two modes of operation. In gas-fueled operation, it is observed that premixed and nonpremixed operation produce nearly the same NO_x levels at low temperatures (below ~1900K). Beyond this, the nonpremixed mode produces higher NO_x emissions. In liquid-fueled operation, the performance is affected by both the temperature as well as the injector placement. The emissions are found to be lower when the liquid injector is retracted into the air annulus compared to when it is level with the air exit. At low adiabatic flame temperatures, the effect is small, but it increases with temperature. To better understand the performance of the combustor in liquid-fueled operation, the remainder of this paper investigates the flowfield and combustion characteristics in this mode of operation through the use of various optical diagnostic techniques.

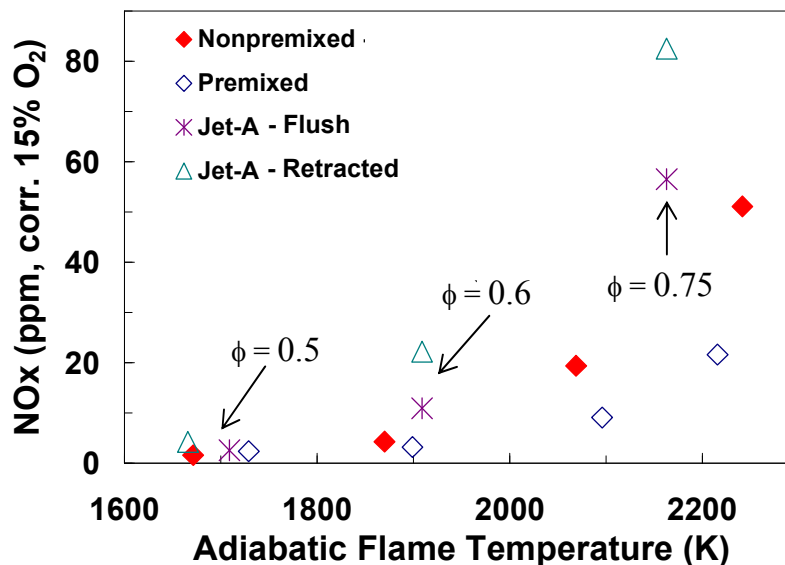


Figure 2. Variation of NO_x with adiabatic flame temperature.

Instantaneous laser scattering images shown in Figure 3 demonstrate the effects of injector placement on fuel dispersion. The distribution of liquid changes significantly depending on the location at which the fuel is injected. When the liquid injector is level with the exit of the air annulus, the fuel enters the combustor as a liquid jet that gradually breaks up to form droplets (Figure 3a). Initially the liquid remains in the center shielded from the returning products by the surrounding air. Further downstream, the jet spreads and significant product entrainment likely occurs, causing the fuel droplets to evaporate. In both injector configurations, droplet scattering images show the presence of a significant amount of liquid at the combustor inlet. Thus, the fuel is not significantly vaporized before entering the combustor, even when it is retracted a few inches.

When the fuel injector is retracted into the air tube (Figure 3b), the liquid fuel enters the combustor in the form of droplets that are spread across the entire width of the injector. Since some of the fuel is now located at the edge of the inlet air jet, it is no longer shielded from the high temperature products, unlike the flush configuration. Thus the liquid fuel close to the product-reactant shear layer can evaporate rapidly, and mix with air and products to form a combustible mixture.

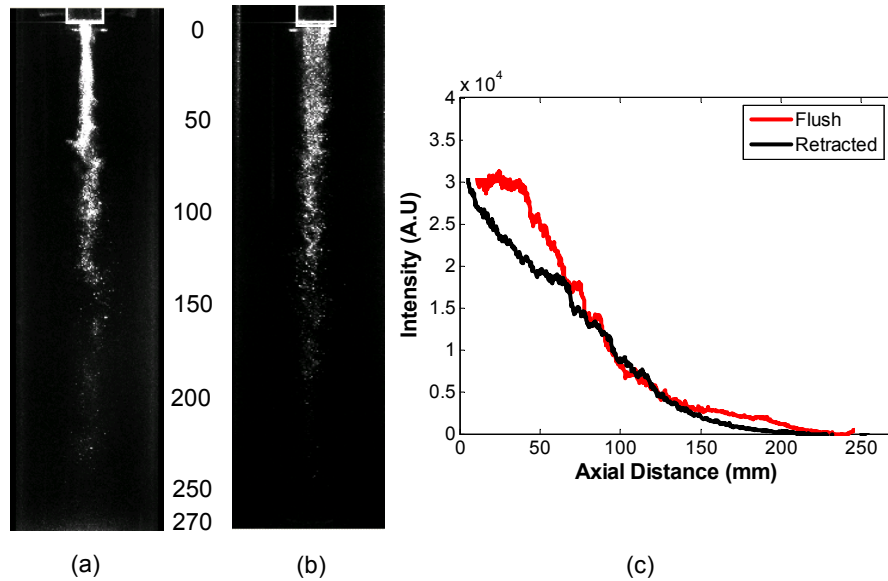


Figure 3. Instantaneous droplet scattering images at $\phi_{\text{global}} = 0.5$ and $m_{\text{air}} = 8\text{g/s}$. (a) Flush (b) Retracted (c) and axial variation of time-averaged, transverse-integrated intensities.

The extent of liquid penetration is determined by plotting the variation in the average droplet intensities (radially integrated across the width of the jet) along the length of the combustor as shown in Figure 3c. For the flush configuration, the average intensity is roughly constant until $\sim 45\text{mm}$, after which it rapidly drops. This behavior is attributed to the dependence of the scattered light intensity on the liquid morphology. Close to the injector exit, the liquid forms a jet that likely undergoes little evaporation. Downstream, as the jet spreads slightly and breaks up to form droplets, the scattered intensity begins to decrease and this continues as the droplets evaporate. Since the jet spread is limited, the downstream drop in scattering intensity is mainly attributed to evaporation rather than dispersion. In contrast, when the liquid injector is retracted, the scattering signal drops more quickly in the upstream portion of the combustor. This is attributed to the dispersion of liquid droplets across the width of the injector causing fuel-product mixing and more rapid evaporation. In this configuration, the scattering image shows that the liquid does not spread radially and hence the drop in intensity downstream is again primarily due to evaporation. On average it is seen that fuel droplets penetrate approximately 220 mm downstream of the injector for both configurations.

Next, the effect of the two different fuel dispersions on the flame characteristics is examined by means of chemiluminescence imaging. Figure 4a,b show the mean CH^* chemiluminescence field for a global equivalence ratio (ϕ_{global}) of 0.5 and an air flow rate of 8 g/s for the flush case and the retracted case. As CH^* is a marker of heat release [8]-[12], the images reveal that the location of the heat release zone varies significantly depending on the position of the fuel injector. Injection of fuel at the exit of the air annulus results in the formation of a highly lifted flame. The lack of heat release near the injector exit is consistent with the fuel distribution seen in Figure 3; with the fuel centrally located and shielded from the hot products, no combustion can occur until further downstream when sufficient evaporation and mixing has occurred. The return flow configuration set by the geometry of the SPRF combustor results in a highly turbulent flowfield causing the flame to exhibit significant radial flapping on an instantaneous basis.

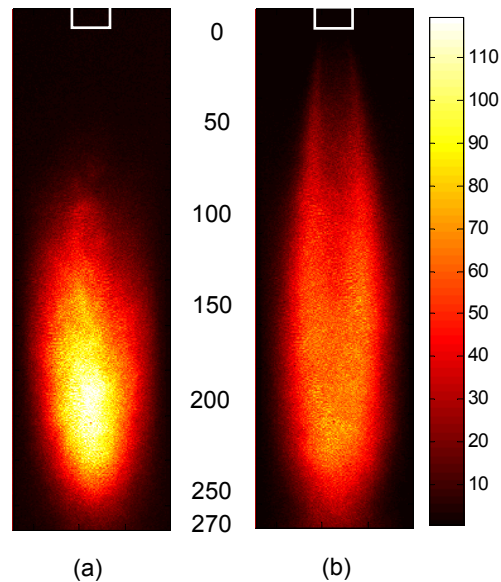


Figure 4. Time-averaged CH* chemiluminescence images for $\phi_{\text{global}}=0.5$ (a) Flush (b) Retracted.

When the liquid is injected further upstream (Figure 4b), heat release can now occur closer to the injector exit because some of the fuel is located along the edge of the inlet jet, where mixing with air and hot products leads to a flammable mixture. The chemiluminescence/heat release in this near-field region is quite low, however, possibly due to a highly strained flame in the shear layer between the incoming reactants and exiting products. Based on analysis of sets of instantaneous images, the flame exhibits less radial flapping in this configuration, but has a greater intermittency close to the injector. Presumably the intermittency is associated with the strain and mixture variability in the shear layer between the reactants and returning products close to the injector exit. A similar shear layer flame region is observed for premixed gas-fueled operation (at the same air mass flow rate).

Based on the averaged chemiluminescence/heat release images, the combustor operating with the retracted liquid injector, with its greater initial fuel dispersion, more closely resembles operation with gaseous fuel when the reactants are premixed (as opposed to when they are nonpremixed). Hence it appears that retracting the fuel injector causes the combustor to operate more like a premixed system.

When ϕ_{global} is raised by increasing the fuel flow rate while maintaining constant air flow, the fuel dispersion and liquid penetration do not change significantly. However the combustion characteristics are altered considerably; the heat release zone becomes shorter and more compact for both injector configurations. As the equivalence ratio increases, the resulting temperature rise causes the overall reactivity of the various species to go up resulting in a shorter more stable flame. On an instantaneous basis the flame does not exhibit significant radial flapping and remains in the central portion of the combustor. Also, for the retracted case, the intermittency close to the injector exit is greatly reduced as ϕ_{global} is increased.

It has been shown that the total chemiluminescence signal integrated over the entire volume of the combustor can be used as an indicator of the overall reaction zone equivalence ratio [13]-[16]. In general, the amount of chemiluminescence from CH* and OH* increases with total fuel flow rate for fixed ϕ and with ϕ for fixed fuel flow rate. For example for Jet-A, the normalized

CH* chemiluminescence intensity (CH^*/m_f) has been predicted to increase monotonically with equivalence ratio for $0.5 < \phi < 1.3$ [17]. The integrated CH* chemiluminescence for the two injector placements is presented in Table 1 for various global equivalence ratios. The integrated CH* signal is consistently lower for the retracted injector case at each ϕ . The lower intensity obtained when the liquid injector is retracted can be interpreted as a leaner overall burning equivalence ratios compared to the flush case (since both cases have the same flow rates). This is also consistent with the observations from the droplet scattering data presented earlier. When the liquid is injected inside the air annulus and the fuel is dispersed across the inlet, vaporization and mixing of air and fuel occur more rapidly than when the fuel is confined within the center of the air jet. The enhanced mixing of vaporized fuel and air leads to leaner fuel-air mixtures in the primary reaction zones, which results in the lower measured NOx emissions.

Table 1. . Integrated CH* chemiluminescence signals

ϕ_{global}	CH*signal (arb units)	
	Flush	Retracted
0.50	2.3	2.2
0.60	8.0	5.3
0.75	18.8	14.6

It is also seen from Table 1 that the change in the integrated signal when the injector is retracted is greater at higher global equivalence ratios. As the temperature increases with ϕ , the enhanced reaction rates lead to a reduction in chemical times. However, as the global equivalence ratio is increased while maintaining a constant air flow rate, the velocities remain nearly the same since the mass flow rate of fuel is negligible compared to that of air. Hence the time scales of mixing remain mostly unaltered as we change the flow condition from $\phi = 0.5$ to $\phi = 0.75$. Over this range of equivalence ratios, the enhanced fuel dispersion produced by the retracted injector leads to lower mixing times compared to the flush case, which helps reduce the overall burning equivalence ratio. At $\phi = 0.5$, this effect is not evident since the lower temperatures prevent reactions from occurring before fuel-air-product mixing has taken place. However as chemical times decrease at higher global equivalence ratios, the lower mixing times facilitated by the retracted injector results in overall leaner burning in the primary reaction zones. Hence, a greater reduction in NOx emissions is obtained for the retracted case at higher ϕ_{global} .

Since NOx formation is greatly influenced by the local temperature distribution in the combustor, it is important to estimate the spatial variation of equivalence ratios produced by the different injector placements. To do this, it is not appropriate to use the integrated CH* or OH* signal since chemiluminescence intensity is also a function of the amount of fuel burned at a given location. This mass dependence is removed by investigating the ratio of CH*/OH* chemiluminescence.

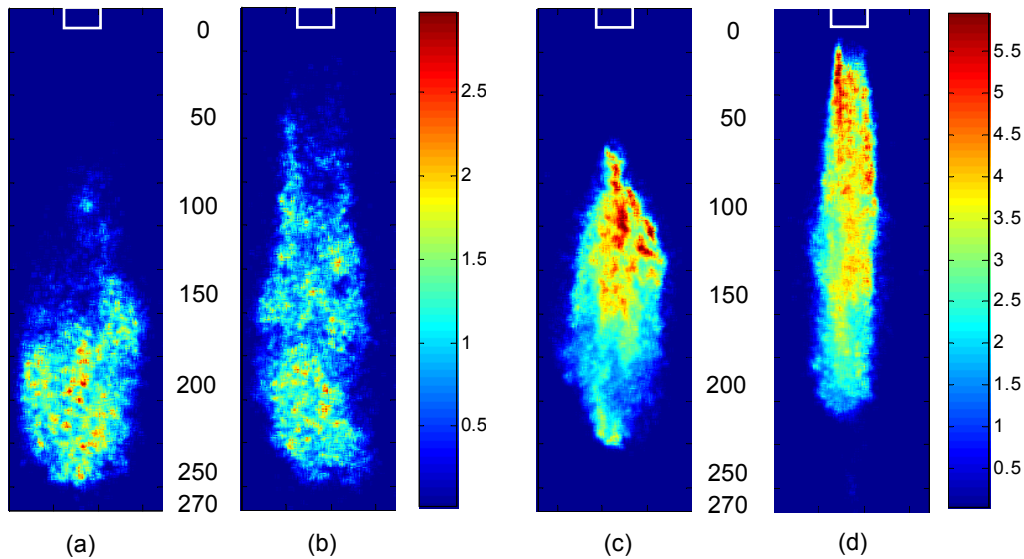


Figure 5. Instantaneous CH*/OH* signal - $\phi_{\text{global}}=0.5$ (a) Flush (b) Retracted $\phi_{\text{global}}=0.75$ (c) Flush (d) Retracted.

Figure 5a,b show instantaneous CH*/OH* ratio images for the two injector configurations at a ϕ_{global} of 0.5. The distribution of CH*/OH* is fairly constant over the entire heat release region in both injector cases. Moreover, the values are nearly the same for the two fuel injector placements, with the flush case having slightly higher ratios. Previous work has shown that CH*/OH* is good indicator of (local) reaction zone equivalence ratio for several fuels [13]-[17]. For methane, this ratio varies monotonically with ϕ , at least for the studied range of $0.7 < \phi < 1.1$. A similar behavior has also been predicted for Jet-A [17]. Hence, it can be inferred that the distribution of equivalence ratios in the combustor is not drastically different for the two injector placements for the $\phi_{\text{global}}=0.5$ case. This is consistent with the NO_x measurements, which show very little variation in the emission levels for the two injector configuration at this operating condition. Also, a majority of the heat release occurs in the regions where CH*/OH* is between 0.5 and 2.

As ϕ_{global} is increased to 0.75 (Figure 5c,d), the CH*/OH* values rise considerably compared to $\phi=0.5$ (Figure 5a,b), i.e., the range of equivalence ratios over which combustion occurs increases as the ϕ_{global} is increased. The flush injector case (Figure 5c) results in somewhat higher local equivalence ratios compared to the retracted case (Figure 5d). Also, the regions of high CH*/OH*, i.e., richer burning regions, is primarily close to the injector for the retracted case while it occurs downstream for the flush case. In both cases, the burning zone equivalence ratio appears to steadily decrease downstream.

Since the overall richer case ($\phi_{\text{global}}=0.75$) appears to have a significant spatial variation in equivalence ratio, it is important to ascertain how the equivalence ratio distribution correlates to the heat release distribution. Figure 6 shows an image of instantaneous CH* chemiluminescence (proportional to heat release) along side the corresponding instantaneous CH*/OH* (proportional to equivalence ratio) for the retracted case at a global equivalence ratio of 0.75. While the near field region has the highest fuel-air ratio, a very small fraction of the heat release occurs close to the injector. Most of the heat release occurs downstream (in the mid region of the combustor),

where the CH*/OH* values are lower, implying leaner combustion. For the flush case, the heat release also occurs in this region, but as seen in Figure 5c, the equivalence ratio of the burning region is still high there. This correlates well with the lower NO_x emissions for the retracted configuration compared to the flush injector.

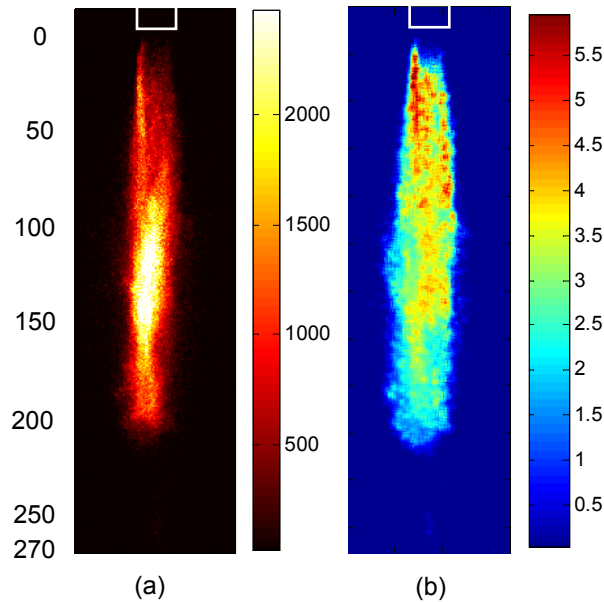


Figure 6. Retracted injector, $\phi_{\text{global}} = 0.75$ (a) Instantaneous CH* chemiluminescence (b) Instantaneous CH*/OH* ratios.

This is further verified by examining all the instantaneous images (typically 250 realizations are obtained for each condition). First however, the CH*/OH* data is converted to a rough estimate of reaction zone equivalence ratio. Nori *et al.* [17] provide modeling results for the CH*/OH* variation with equivalence ratio for Jet-A based on detailed chemical kinetic modeling. Their results are calibrated to the current measurement system using the results from the $\phi=0.5$ measurements, where the burning equivalence ratio appears to be nearly uniform and only slightly richer than the overall ϕ .

Figure 7 shows histograms of the fraction of image area (i.e., pixels in which a chemiluminescence/heat release signal is present) that correspond to four equivalence ratio ranges ($\phi < 0.68$, $0.68 \leq \phi < 0.83$, $0.83 \leq \phi < 1$, $1 \leq \phi$). Also shown is a histogram of the fraction of heat release (from the CH* images) associated with each equivalence ratio range. Results are presented for three global equivalence ratios and for both injector locations.

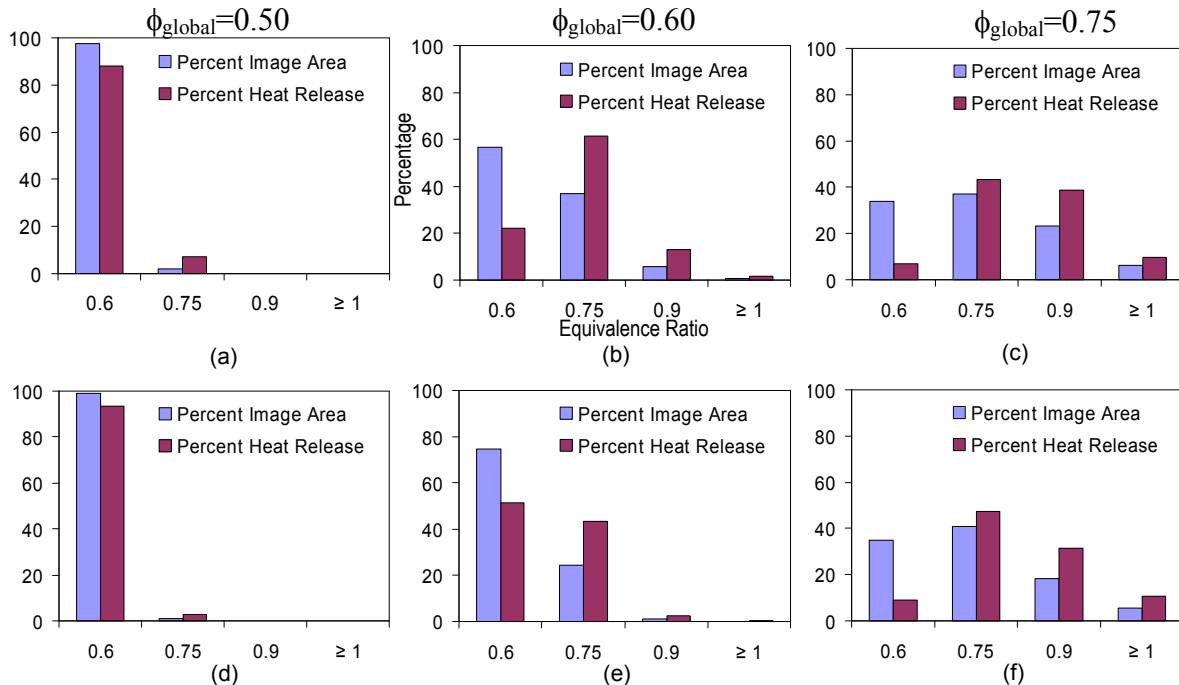


Figure 7. Histogram of the fractional heat release occurring at different equivalence ratios: (a), (b), (c) - Flush case (d), (e), (f) - Retracted case.

As ϕ_{global} is increased, the results show that the range of local equivalence ratios measured in the combustor also increases. As noted previously for the leanest case ($\phi_{global}=0.5$), the variations of reaction zone equivalence ratios for the flush injector (Figure 7a) and retracted injector (Figure 7d) are small. Moreover, the majority of the heat release occurs in the same narrow range, though the flush case does show a slightly higher fraction of heat release at local ϕ values near 0.75. For $\phi_{global}=0.6$, the heat release is spread over a broader range of equivalence ratios. From Figure 7b and 7e, it is seen that most (>80%) of the heat release occurs for local ϕ 's below ~ 0.8 . In the retracted configuration, the heat release is shifted to lower fuel-air mixtures, with $\sim 50\%$ occurring below $\phi=0.7$ and $\sim 90\%$ of the heat release associated with $\phi < 0.8$. In contrast for the flush case, 10-15% of the heat release occurs at closer to stoichiometric conditions ($\phi > 0.8$). These small regions of high local fuel-air ratio are the likely source of the higher measured NOx emissions for the flush injector configuration. For the highest global equivalence ratio case (0.75), both injector configurations (Figure 7c and 7f) have more than 40% of the heat release occurring in regions where the local $\phi > 0.8$. Again, the flush injector has a slightly higher fraction of heat release associated with near stoichiometric local conditions. Since the NOx penalty associated with near stoichiometric conditions is very high, even this slight increase in burning zone equivalence ratio distribution can result in the significant increase in measured NOx emissions for the flush case at $\phi_{global}=0.75$. Therefore the improved fuel dispersion for the retracted injector results in a reduction in equivalence ratios in the primary heat release zone leading to lower NOx emissions over the entire range of global equivalence ratios.

4. Concluding Remarks

The combustion characteristics of a SPRF combustor operating with liquid fuel (Jet-A) have been investigated with respect to the variation in NO_x emissions for different fuel injector configurations. Non-intrusive optical diagnostic techniques including laser droplet scattering and chemiluminescence imaging are employed to analyze the fuel distribution and to characterize the heat release and reaction zone equivalence ratio distribution in the combustor.

The effect of fuel distribution on the flowfield of the combustor was investigated by varying the upstream location at which the liquid fuel is injected, thus altering the spray pattern as well as the extent of fuel-product shielding in the combustor. When the liquid injector is flush with the air annulus, fuel enters the combustor in the form of a liquid jet surrounded by the annular air stream. Shear provided by the high velocity annular air flow facilitates atomization of the liquid jet and also shields it initially from the high temperature return flow. In this configuration, heat release is limited by the rate of evaporation of the liquid and we see a highly lifted flame where most of the heat release occurs in the central portion of the combustor. Retraction of the liquid injector well into the air annulus results in better dispersion of the fuel across the inlet air jet. In this configuration, although the fuel is no longer shielded from the hot products, the enhanced dispersion eventually results in the formation of a leaner mixture of fuel, air and products in the primary reaction zones; thus NO_x emissions are reduced. This is supported by the chemiluminescence measurements, interpreted two ways: first by the global/integrated chemiluminescence signal (which decreases as the fixed total heat release occurs at a lower average reaction zone equivalence ratio), and second by CH*/OH* ratios that show that the regions of high heat release are associated with lower reaction zone equivalence ratios in the retracted injector case.

At very lean conditions, there is little difference between the NO_x emissions or reaction zone equivalence ratios for the two injector configurations. This suggests that there is sufficient time in both configurations for evaporated fuel to mix well with the air before combustion occurs. However, as the global equivalence ratio (based on input fuel and air) increases the well dispersed fuel in the retracted case results in lower reaction zone equivalence ratios and lower NO_x emissions than for the flush injector. For the higher ϕ_{global} cases, the combustor temperature rises, and therefore the characteristic chemical (τ_{chem}) and evaporation (τ_{evap}) times for the reactant/product mixtures decrease with an increase in ϕ_{global} . Since the current experiments maintained the overall flowrate nearly constant, we expect the mixing times to be a weaker function of ϕ_{global} , i.e., $\tau_{\text{mix}} \approx \text{constant}$. Thus the effective Damkohler number ($Da = \tau_{\text{mix}} / \tau_{\text{chem}}$) for the combustor likely increases with ϕ_{global} . As Da increases, eventually there will not be enough time for good fuel-air mixing to occur before reactions begin, and the fuel will burn at local equivalence ratios significantly richer than ϕ_{global} . This is what we observe. Since the retracted injector disperses the fuel better, it reduces τ_{mix} compared to the flush case, and therefore it is able to produce leaner reaction zone equivalence ratios at a given ϕ_{global} compared to the flush injector.

Therefore it is this interaction of the chemical times, evaporation rates and mixing times that controls the NO_x performance of the combustor in liquid operation. While low NO_x levels in nonpremixed gas-based operation have been attributed to complete shielding of fuel from products when they enter the combustor, it is observed in liquid-fueled operation that the added

delay caused by fuel evaporation before mixing and combustion can occur, changes this fuel-product shielding requirement.

Acknowledgments

This research was supported by NASA through the University Research, Engineering, and Technology Institute for Aeropropulsion and Power, under Grant/Cooperative Agreement Number NCC3-982.

References

- [1] Y. Neumeier, B. Zinn, Y. Weksler, J. Seitzman, J. Jagoda, and J. Kenny: AIAA-2005-3775 Joint Propulsion Conference, July 2005 Tucson, Arizona.
- [2] J. Crane, Y. Neumeier, J. Jagoda, J. Seitzman and B. Zinn : GT2006-91338, Proceedings of ASME/IGTI Turbo Expo 2006, May 8-11, 2006 Barcelona, Spain.
- [3] M. K. Bobba, P. Gopalakrishnan, A. Radhakrishnan, J. Seitzman, Y. Neumeier, B. Zinn, and J. Jagoda: AIAA-2006-963 44th AIAA Aerospace Sciences Meeting and Exhibit, Jan. 9-12, 2006 Reno, Nevada.
- [4] P. Gopalakrishnan, S. Undapalli, M. Bobba, V. Sankaran, S. Menon, B. T. Zinn, and J. M. Seitzman: AIAA-2006-962 44th AIAA Aerospace Sciences Meeting and Exhibit, Jan. 9-12, 2006 Reno, Nevada.
- [5] V. Sankaran, P. Gopalakrishnan, S. Undapalli, V. Parisi, J. M. Seitzman, and S. Menon: AIAA2005-3969 41st AIAA/ASME/SAE/ASEE Joint Propulsion Conference & Exhibit 10 - 13 July 2005, Tucson, Arizona.
- [6] M. K. Bobba, P. Gopalakrishnan, J. M. Seitzman and B. T. Zinn: GT2006-91217, Proceedings of ASME/IGTI Turbo Expo 2006, May 8-11, 2006 Barcelona, Spain.
- [7] P. Gopalakrishnan, M. K. Bobba and J.M. Seitzman: Proc. of Comb. Inst.(2006).
- [8] C. J. Lawn: *Combustion and Flame* 132 (2000) 227-240.
- [9] R. J. Roby, A. J. Hamer, E. L. Johnsson, S. A. Tilstra and T. J. Burt: *Transactions of the ASME* 117 (1995) pp332 –340.
- [10] H. N. Najm, P. H. Paul, C. J. Mueller and P. S. Wyckoff: *Combustion and Flame* 113 (3) (1998) 312-332.
- [11] G. K. Mehta, M. K. Ramachandra and W. C. Strahle: *Proc. Combust. Inst.* 18 (1980) 1051-1059.
- [12] J. Kojima, Y. Ikeda and T. Nakajima: Twenty eighth Symposium (International) on Combustion, 2000, pp. 1757-1764.
- [13] R. J. Roby, J. E. Reaney and E. L. Johnsson: Proceedings of the 1998 Int. Joint Power Generation Conference, Vol. 1, 1998, 593-602.
- [14] Y. Ikeda, J. Kojima and T. Nakajima: AIAA-2002-0191, 40th Aerospace sciences meeting and exhibit, Reno, Nevada, Jan 14-17, 2002.
- [15] M. R. Morrell, J. M. Seitzman, M. Wilensky, E. Lubarsky and B. Zinn: AIAA 2001-0787 39th AIAA Aerospace Sciences Meeting and Exhibit, Jan. 8-11, 2001 Reno, Nevada.
- [16] T. M. Muruganandam, B.-H. Kim, M. R. Morrell , V. Nori, M. Patel, B. W. Romig and J. M. Seitzman, Proc. Combust. Inst. 30, pp. 1601-1609, The Combustion Institute (2005).
- [17] V. N. Nori and J. M. Seitzman: AIAA-2007-0466, 45th Aerospace Sciences Meeting, Reno, NV, Jan 8-11, 2007.